


## Article

# High-Throughput Computational Screening of Ionic Liquids for Butadiene and Butene Separation

Hao Qin <sup>1</sup>, Zihao Wang <sup>2</sup>, Zhen Song <sup>1,3</sup>, Xiang Zhang <sup>2,\*</sup> and Teng Zhou <sup>1,2,\*</sup> 
<sup>1</sup> Process Systems Engineering, Otto-von-Guericke University Magdeburg, Universitätsplatz 2, D-39106 Magdeburg, Germany; qin@mpi-magdeburg.mpg.de (H.Q.); songz@ecust.edu.cn (Z.S.)

<sup>2</sup> Process Systems Engineering, Max Planck Institute for Dynamics of Complex Technical Systems, Sandtorstr. 1, D-39106 Magdeburg, Germany; zwang@mpi-magdeburg.mpg.de

<sup>3</sup> School of Chemical Engineering, East China University of Science and Technology, 130 Meilong Road, Shanghai 200237, China

\* Correspondence: zhangx@mpi-magdeburg.mpg.de (X.Z.); zhout@mpi-magdeburg.mpg.de (T.Z.)

**Abstract:** The separation of 1,3-butadiene (1,3-C<sub>4</sub>H<sub>6</sub>) and 1-butene (n-C<sub>4</sub>H<sub>8</sub>) is quite challenging due to their close boiling points and similar molecular structures. Extractive distillation (ED) is widely regarded as a promising approach for such a separation task. For ED processes, the selection of suitable entrainer is of central importance. Traditional ED processes using organic solvents suffer from high energy consumption. To tackle this issue, the utilization of ionic liquids (ILs) can serve as a potential alternative. In this work, a high-throughput computational screening of ILs is performed to find proper entrainers, where 36,260 IL candidates comprising of 370 cations and 98 anions are involved. COSMO-RS is employed to calculate the infinite dilution extractive capacity and selectivity of the 36,260 ILs. In doing so, the ILs that satisfy the prespecified thermodynamic criteria and physical property constraints are identified. After the screening, the resulting IL candidates are sent for rigorous process simulation and design. 1,2,3,4,5-pentamethylimidazolium methylcarbonate is found to be the optimal IL solvent. Compared with the benchmark ED process where the organic solvent N-methyl-2-pyrrolidone is adopted, the energy consumption is reduced by 26%. As a result, this work offers a new IL-based ED process for efficient 1,3-C<sub>4</sub>H<sub>6</sub> production.

**Keywords:** butadiene/butene separation; ionic liquid; high-throughput screening; extractive distillation; COSMO-RS



**Citation:** Qin, H.; Wang, Z.; Song, Z.; Zhang, X.; Zhou, T. High-Throughput Computational Screening of Ionic Liquids for Butadiene and Butene Separation. *Processes* **2022**, *10*, 165. <https://doi.org/10.3390/pr10010165>

Academic Editor: Giancarlo Cravotto

Received: 22 December 2021

Accepted: 13 January 2022

Published: 15 January 2022

**Publisher's Note:** MDPI stays neutral with regard to jurisdictional claims in published maps and institutional affiliations.



**Copyright:** © 2022 by the authors. Licensee MDPI, Basel, Switzerland. This article is an open access article distributed under the terms and conditions of the Creative Commons Attribution (CC BY) license (<https://creativecommons.org/licenses/by/4.0/>).

## 1. Introduction

1,3-Butadiene (1,3-C<sub>4</sub>H<sub>6</sub>) is an important petrochemical-based raw material for producing polybutadiene, which is one of the most important synthetic rubbers. In 2015, 11 million metric tons of 1,3-C<sub>4</sub>H<sub>6</sub> valued at 30–40 billion dollars were produced [1]. The increasing demand and giant market potential of 1,3-C<sub>4</sub>H<sub>6</sub> led to widespread attention to its efficient production from both academia and industry. Typically, pure 1,3-C<sub>4</sub>H<sub>6</sub> stream can be isolated from the C<sub>4</sub> hydrocarbon mixtures that are generated from the steam cracking processes for ethylene generation. 1,3-C<sub>4</sub>H<sub>6</sub> accounts for 30–60% of the C<sub>4</sub> mixtures and the rest are mainly comprised of 1-butene (n-C<sub>4</sub>H<sub>8</sub>), isobutene (iso-C<sub>4</sub>H<sub>8</sub>), and butane (C<sub>4</sub>H<sub>10</sub>) [2–4]. Within the C<sub>4</sub> mixture, the close boiling points between 1,3-C<sub>4</sub>H<sub>6</sub> (268.75 K) and n-C<sub>4</sub>H<sub>8</sub> (266.65 K) as well as their similar molecular structures cause great difficulties in the separation process by means of simple distillation. To overcome this challenge, an effective and efficient separation technique is highly desired.

It is well known that the extractive distillation (ED) process offers an efficient option for separating close-boiling mixtures. A proper entrainer can be introduced to significantly increase the relative volatility of the target component for enhancing the separation efficiency [5–8]. The polar aprotic solvents such as N-methyl-2-pyrrolidone (NMP),

dimethylformamide (DMF) and acetonitrile (ACN) are usually used in the industry. Nevertheless, when those organic solvents are used for  $C_4$  separation, the associated processes are featured by a high solvent/feed ratio, requiring a large amount of energy for solvent recovery [8–10]. Thus, it is highly favored to design an energy-saving ED process from the economic point of view. In this case, the selection of a suitable entrainer is always crucial [11–13].

Ionic liquids (ILs), a category of neoteric solvent, are defined as molten salts with melting points below 100 °C. Due to their unique physicochemical properties, such as excellent solvation ability, wide liquid range, extremely low vapor pressure and flexible designability, ILs have received extensive attention for use in various applications [14–21]. Numerous studies have been reported for optimal design of ILs-based ED processes to separate azeotropic or close-boiling mixtures such as alcohol/water, alcohol/aliphatic hydrocarbons, aromatic/aliphatic hydrocarbons, etc. [22–26]. Despite the progress made, the investigation of ILs for separating 1,3- $C_4H_6$  and n- $C_4H_8$  is still limited. The existing studies focused on the experimental trial-and-error approaches (see references [27–31]). However, due to a large pool of diverse cation–anion combinations, the experimental procedure is time-consuming and costly. Importantly, only a small design space can be covered. Therefore, a reliable and efficient theoretical method is needed to identify the optimal ILs.

For efficient IL screening, the reliable prediction of thermodynamic properties of IL-containing systems is a prerequisite. To this end, COSMO-RS (Conductor-like Screening Model for Real Solvents) has been demonstrated to be a promising tool for predicting the thermodynamic properties of IL-containing systems accurately. Other than the activity coefficient models (e.g., NRTL, UNIFAC, UNIQUAC) [32–36] and equation of state methods (e.g., SAFT) [37] that strongly rely on experimentally fitted parameters, COSMO-RS is a fully predictive thermodynamic model that combines quantum chemistry with statistical thermodynamics to generate reliable predictions. COSMO-RS is elucidated to be a versatile platform for fast IL screening with a given separation task, presenting good qualitative and, in many cases, acceptable quantitative prediction results [38–42]. Specifically for hydrocarbon systems involving ILs, COSMO-RS is verified to be robust for describing the phase behaviors (see references [43–46]). That is to say, it is advisable to apply COSMO-RS as the IL screening tool for 1,3- $C_4H_6$  recovery.

In this work, a high-throughput computational screening of ILs is performed for 1,3- $C_4H_6$  and n- $C_4H_8$  separation. Two systematic steps are incorporated. The first step accounts for IL screening based on predefined constraints on thermodynamic and physical properties. Thermodynamic evaluation based on the COSMO-RS is conducted to calculate infinite dilution capacity and selectivity of IL candidates. In addition, the physical properties (i.e., viscosity, toxicity and melting point) of ILs are estimated using available property prediction models. After the screening, the resulted IL candidates are sent to identify their explicit process performance. Process performance evaluation is carried out using Aspen Plus simulation (V8.8). As a result, [PMIM][MC] is optimally identified from 36,260 ILs, denoting much lower energy consumption in comparison with the benchmark ED process using NMP.

## 2. Methods Description

### 2.1. Thermodynamic Evaluation by COSMO-RS

Two major steps for COSMO-RS calculation are briefly illustrated here: first, through the standard quantum chemical computation, the screening charge density distributions (i.e.,  $\sigma$ -profiles) for the compound of interest can be determined; second, the compound chemical potential is quantified from the statistical thermodynamics treatment of molecular interactions with the obtained  $\sigma$ -profiles. Consequently, the prediction of thermodynamic properties such as activity coefficient is feasible on account of the chemical potential of an arbitrary solute in any pure or mixed solvent.

COSMO-RS allows for the calculation of activity coefficient according to Equation (1):

$$\gamma_S^i = \exp \left\{ \frac{\mu_S^i - \mu_i^i}{RT} \right\} \quad (1)$$

where  $\mu_S^i$  and  $\mu_i^i$  are the chemical potentials of solute  $i$  in the solvent  $S$  and pure compound  $i$ , respectively. With this, the extractive capacity  $C^\infty$  and selectivity  $S^\infty$  at infinite dilution can be calculated accordingly:

$$C^\infty = (1/\gamma_i^\infty)^{IL} \quad (2)$$

$$S^\infty = (\gamma_j^\infty/\gamma_i^\infty)^{IL} \quad (3)$$

where  $\gamma_i^\infty$  and  $\gamma_j^\infty$  denote the infinite dilution activity coefficient of solute  $i$  and dilute  $j$  in an IL, respectively.  $C^\infty$  and  $S^\infty$  could reflect the extractive potential of a solvent with a specific separation task, which are widely adopted and proven to be useful in the literature [47–50]. In this study, the infinite dilution activity coefficient of 1,3-C<sub>4</sub>H<sub>6</sub> and n-C<sub>4</sub>H<sub>8</sub> in the 36,260 ILs (i.e.,  $\gamma_1^\infty$  and  $\gamma_2^\infty$ ) are directly calculated using COSMO-RS (Version 19.0.5) with the BP\_TZVP\_C30\_1901 parameterization. The 370 cations cover different cation families such as imidazolium, pyridinium, pyrrolidinium, piperidinium, ammonium and phosphonium, which are combined with 98 anions such as acetate, methylcarbonate, chloride, lactate, bis(trifluoromethylsulfonyl)imide, hexafluorophosphate, etc. The information about the involved cations and anions are tabulated in Table S1 (Supplementary Materials). The COSMO files of cations, anions and C<sub>4</sub> hydrocarbons are taken from the COSMO-RS database. Based on the auxiliary batch-processing program in COSMOthermX (i.e., CT\_CREATE), a template input file is needed for enabling an efficient computation. In addition, the infinite dilution activity coefficient of four commercial organic solvents (i.e., NMP, DMF, DMSO and ACN) can be calculated. Regarding the organic solvent as benchmark solvents, the  $C^\infty$  and  $S^\infty$  of IL candidates are directly compared with those of the four organic solvents to sort out the promising ILs with better thermodynamic performance for 1,3-C<sub>4</sub>H<sub>6</sub> recovery.

## 2.2. Physical Properties Assessment

The ILs that satisfy the thermodynamic criteria should go through the physical property assessments from the perspective of practical application. Referring to the work by Eiden et al. [51], COSMO-RS is employed to predict the IL viscosity as a QSPR approach. The specific equation is written as:

$$\ln \left( \frac{\eta}{\eta_0} \right) = a \ln(r_m) + b E_{diel} + c \sigma' + d \quad (4)$$

where  $r_m$  is the mean IL radius,  $E_{diel}$  is the sum of dielectric energies of the cation and anion, and  $\sigma'$  is the symmetry factor. To ensure that ILs can flow easily, the IL viscosity constraint is set to be:

$$\eta < 150 \text{ cP} \quad (5)$$

As the underlying hazards of ILs have gradually been recognized in recent years, the IL toxicity should be taken into account [52–54]. The EC<sub>50</sub> (half-maximal effective concentration) of ILs against IPC-81 (Leukemia rat cell line) is considered and predicted using two machine learning (ML) models proposed by Wang et al. The two ML models consist of the feedforward neural network (FNN) and support vector machine (SVM) models [54]. According to the criteria proposed by the UFT research unit from the University of Bremen, the cytotoxicity of ILs towards IPC-81 can be divided into four categories; that is, very high (EC<sub>50</sub> < 1.0), high (1.0 < EC<sub>50</sub> < 100), moderate (100 < EC<sub>50</sub> < 5000) and low (EC<sub>50</sub> > 5000). Therefore, log<sub>10</sub>EC<sub>50</sub> < 2 indicates a high toxicity, which should be avoided.

$$\log(\text{EC}_{50}) \geq 2 \quad (6)$$

Moreover, the IL melting point is estimated using the GC model developed by Lazzús et al. [55], as expressed by:

$$T_m(K) = 288.7 + \sum_{i=1}^{31} n_i \Delta t_{ci} + \sum_{j=1}^{36} n_j \Delta t_{aj} \quad (7)$$

where  $n_i$  and  $n_j$  are the numbers of the cation group  $i$  and anion group  $j$  in IL, respectively.  $\Delta t_{ci}$  and  $\Delta t_{aj}$  are the contributions of the cation and anion groups to the melting point, respectively. The melting point of ILs is set to be lower than 298.15 K to ensure the screened ILs are liquid under room temperature.

$$T_m(K) < 298.15 \quad (8)$$

### 2.3. Process Simulation

Aspen Plus V8.8 is employed to simulate the ED process for separating 1,3-C<sub>4</sub>H<sub>6</sub> and n-C<sub>4</sub>H<sub>8</sub>. The organic solvent NMP is first used as entrainer. The corresponding ED process serves as the benchmark process for easy comparison. The components of NMP, 1,3-C<sub>4</sub>H<sub>6</sub> and n-C<sub>4</sub>H<sub>8</sub> are directly available in the Aspen databank. For IL-containing systems, since ILs are not included in the Aspen databank, they are defined as pseudo-components by specifying their molecular weights (MW), normal boiling points (NBP) and densities. The NBP of ILs is estimated by the fragment contribution-corresponding states (FC-CS) method proposed by Huang et al. [56]. The densities and molecular weights are acquired from the COSMO-RS calculation. Note that when NMP is utilized, the NRTL model is selected with the binary parameters retrieved directly from the Aspen database. For the IL process, COSMO-SAC is adopted as the thermodynamic model. Six parameters of molecular volume (CSACVL) and sigma profiles (SGPRF1 to SGPRF5) are calculated by COSMO-RS and specified in Aspen Plus. For modeling the distillation column, the RadFrac block is used where the equilibrium stage model is employed and total condenser and kettle reboiler are selected.

## 3. Results and Discussion

### 3.1. Screening of ILs via Thermodynamic Evaluation

The  $\gamma_1^\infty$  and  $\gamma_2^\infty$  in the 36,260 ILs at 298.15 K were predicted by COSMO-RS as summarized in Table S2 (Supplementary Materials). Consequently, the capacity  $C^\infty$  and selectivity  $S^\infty$  were calculated to assess the extraction ability of ILs. It was found that 36,180 ILs had selectivity towards 1,3-C<sub>4</sub>H<sub>6</sub> above 1, which suggests the great potential of ILs as the entrainer to separate 1,3-C<sub>4</sub>H<sub>6</sub> from n-C<sub>4</sub>H<sub>8</sub>. In order to visualize the calculation results, the relationship between  $C^\infty$  and  $S^\infty$  for the 36,180 ILs is plotted in Figure 1. Clearly, as the selectivity increases, the capacity decreases. Due to such a tradeoff, simultaneous consideration of selectivity and capacity is required.

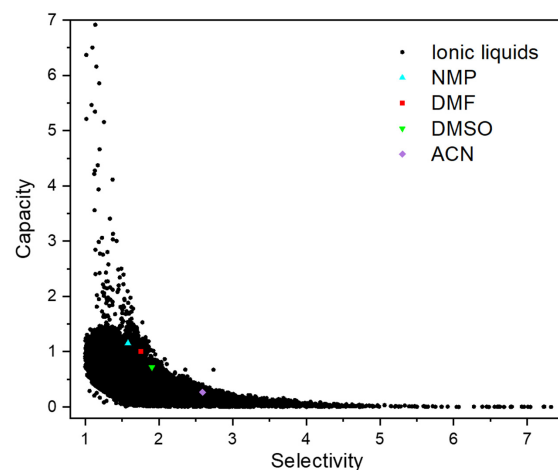


**Figure 1.** Infinite dilution capacity and selectivity of ILs and reference solvents calculated by COSMO-RS at 298.15 K.

The capacity and selectivity of NMP, DMF, DMSO and ACN are also depicted in Figure 1. Obviously, many ILs have larger capacity and selectivity than these four organic solvents. A boundary front was regressed based on the four solvents to explicitly screen ILs. As shown in Figure 2, two empirical selection criteria were defined to exclude the ILs with moderate performance. The first was that the capacity difference between the promising ILs and the boundary front should be larger than 0.1. The second was that the selectivity of ILs should be between those of NMP and ACN. Accordingly, as listed in Table S3 (Supplementary Materials), 190 out of 36,180 ILs met the two thermodynamic criteria and thus were retained.

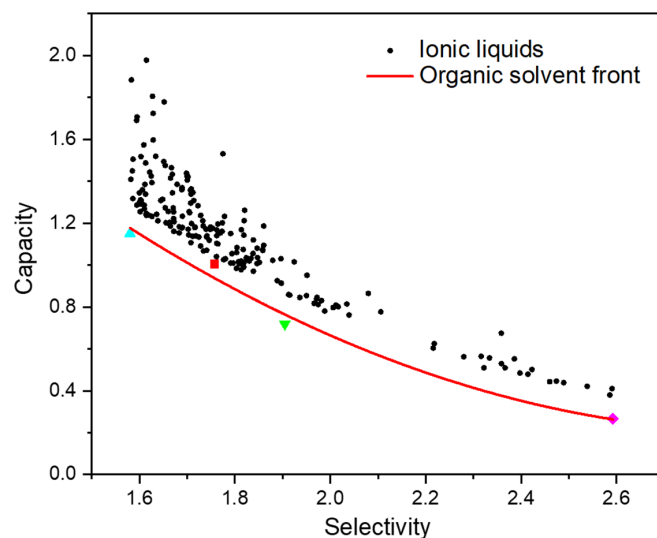


**Figure 2.** Screening of ILs with better extraction performance in contrast with the reference solvents (capacity of IL > capacity of organic solvents + 0.1).

### 3.2. Screening of ILs via Physical Property Constraints

The  $\eta$ , log EC50 and  $T_m$  of the 190 ILs were further checked and the results are given in Table S4 (Supplementary Materials). Given the physical property constraints of Equations (5), (6) and (8), it was found that only one IL [PMIM][MCO] satisfied the three physical property constraints in Section 2.2. [PMIM][MCO] comprises of 1,2,3,4,5-pentamethylimidazolium (cation No. 48) and methylcarbonate (anion No. 64). Its melting point and viscosity were 260.34 K and 136.37 cp, respectively. In addition, the logEC50 values were 3.19 and 3.37, predicted by the FNN and SVM model, respectively. In this case, [PMIM][MCO] is regarded as a promising solvent for separating 1,3-C<sub>4</sub>H<sub>6</sub> and n-C<sub>4</sub>H<sub>8</sub>. The structure information of [PMIM][MCO], along with the benchmark solvent NMP, is shown in Figure 3. Both were subsequently employed and compared as the entrainer for the ED process simulation.

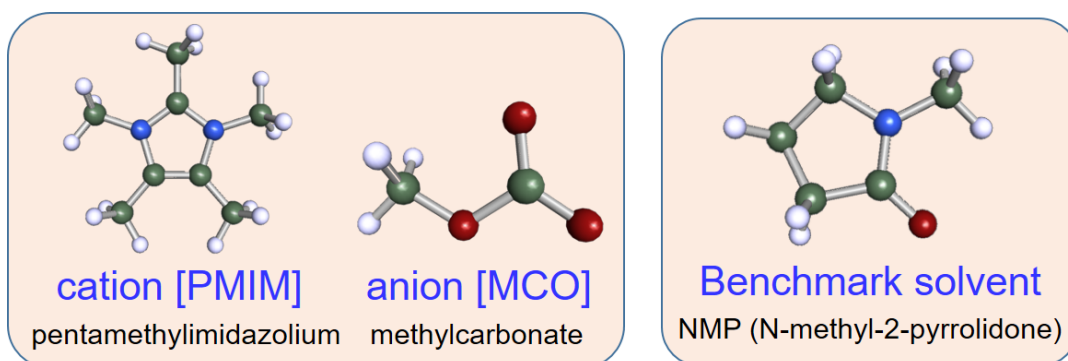


**Figure 3.** Structure information of the screened IL and the benchmark solvent NMP.

### 3.3. Final Evaluation by Process Simulation

After the identification of the optimal IL, the ED process was simulated in Aspen Plus V8.8 for 1,3- $\text{C}_4\text{H}_6$ /n- $\text{C}_4\text{H}_8$  separation. The schematic diagram of the ED process is illustrated in Figure 4. It consisted of an extractive distillation column and a solvent recovery column. Typically, the entrainer was fed to the top of the extractive distillation column. A suitable feeding stage was investigated. The light component n- $\text{C}_4\text{H}_8$  was withdrawn from the distillate, whereas the heavy component 1,3- $\text{C}_4\text{H}_6$  together with the entrainer left from the bottom. The heavy component and entrainer were subsequently separated in the solvent recovery column. Ultimately, the high-purity 1,3- $\text{C}_4\text{H}_6$  and entrainer were collected from the top and the bottom of the solvent recovery column, respectively. The flow rates of 1,3- $\text{C}_4\text{H}_6$  and n- $\text{C}_4\text{H}_8$  in the feed stream were set equally at 50 kmol/h. In addition, the two columns were operated with the atmospheric pressure. Moreover, when the benchmark solvent NMP was adopted, all the related parameters were retrieved from the Aspen databank. When the optimal IL [PMIM][MCO] was utilized, all the input information needed (e.g., molecular weight, normal boiling point, and density of the IL as well as parameters of CSACVL and SGPRF1 to SGPRF5 for the COSMO-SAC model in Aspen Plus) were recorded in Table S5 (Supplementary Materials).

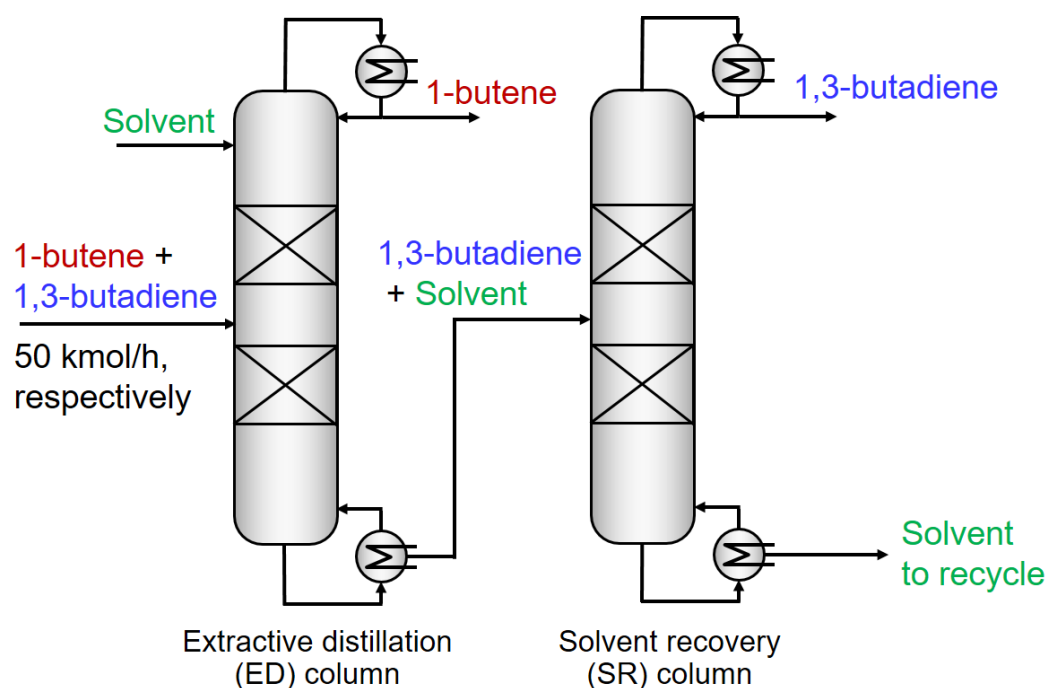


**Figure 4.** Flowsheet of the ED process for 1,3- $\text{C}_4\text{H}_6$  and n- $\text{C}_4\text{H}_8$  separation.

Based on the above process, preliminary simulations with different operating conditions were performed and it was found that the most important operating parameters were the solvent flow rate and the reflux ratio in the extractive distillation column. Therefore, these two critical operating conditions are regarded as process design variables. The other operating conditions (see Table 1) were simply fixed and the parameter sensitivity analysis was conducted on the two design variables in order to find the optimal operating conditions for minimizing the total reboiler duty of the two columns. Meanwhile, a 99.5% molar product (1,3-butadiene) purity was ensured. Given the optimal IL, Figure 5a,b illustrates the influences of the two process design variables on product purity and total reboiler duty, respectively. Similarly, Figure 6a,b shows the impacts of the two design variables when the NMP was used. The feasible operating areas that succeeded in meeting the separation task of 99.5% product purity are denoted as the red region. After comparing Figures 5 and 6, it was found that for the IL-based process, the feasible area was larger and closer to the left



lower corner. This means that a lower solvent usage and reflux ratio are required. This proves the advantage of the optimal IL.

**Table 1.** Fixed conditions after the preliminary Aspen-based process investigations.

Parameters	Column	NMP-Based Process	IL-Based Process
Total number of stages	ED	40	40
	SR	5	4
Feed location	ED	20	20
	SR	3	2
Reflux ratio	SR	0.5	0.0001

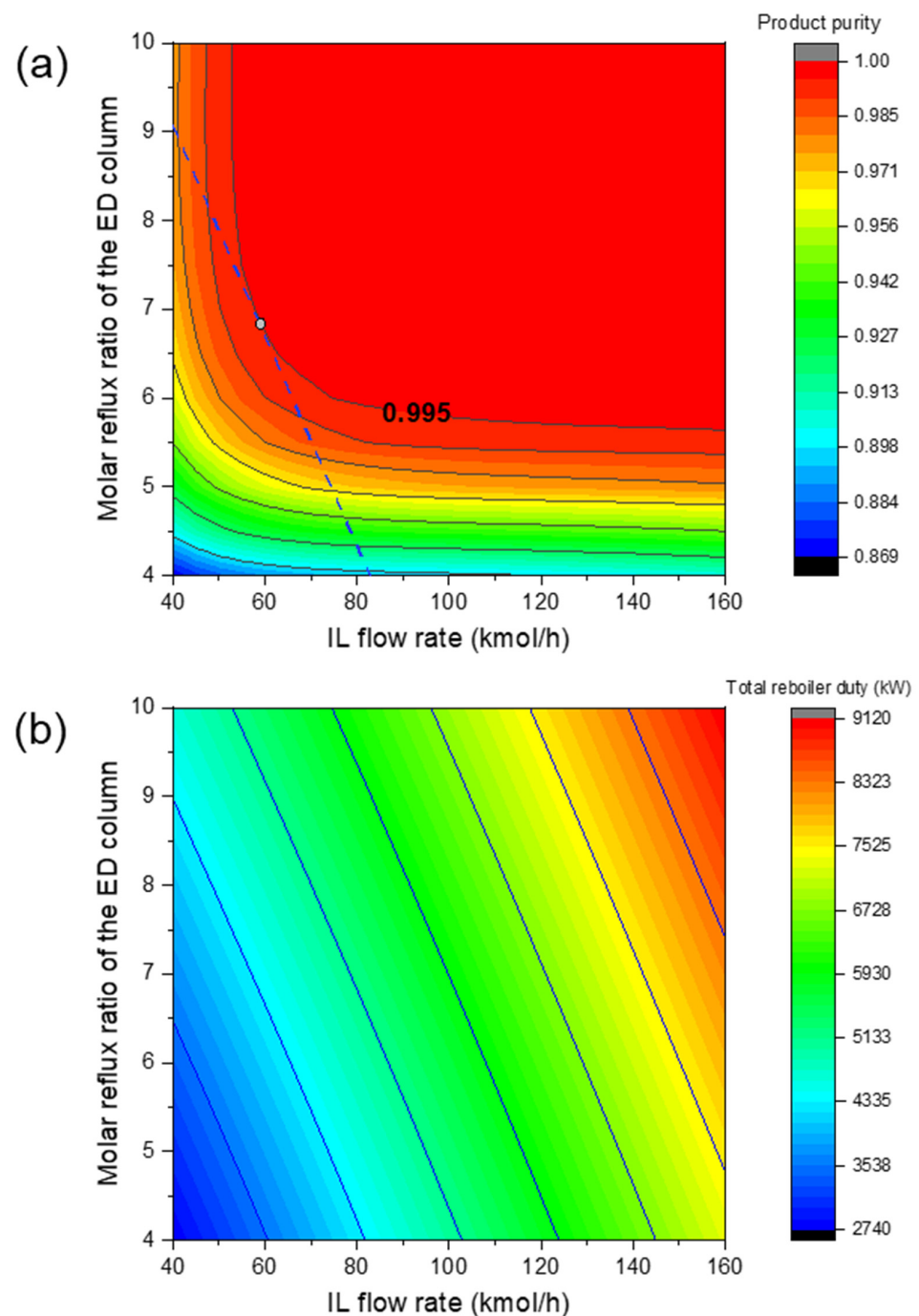


**Figure 5.** Influence of reflux ratio of the ED column and solvent usage on (a) product purity and (b) total reboiler duty for the IL-based process.

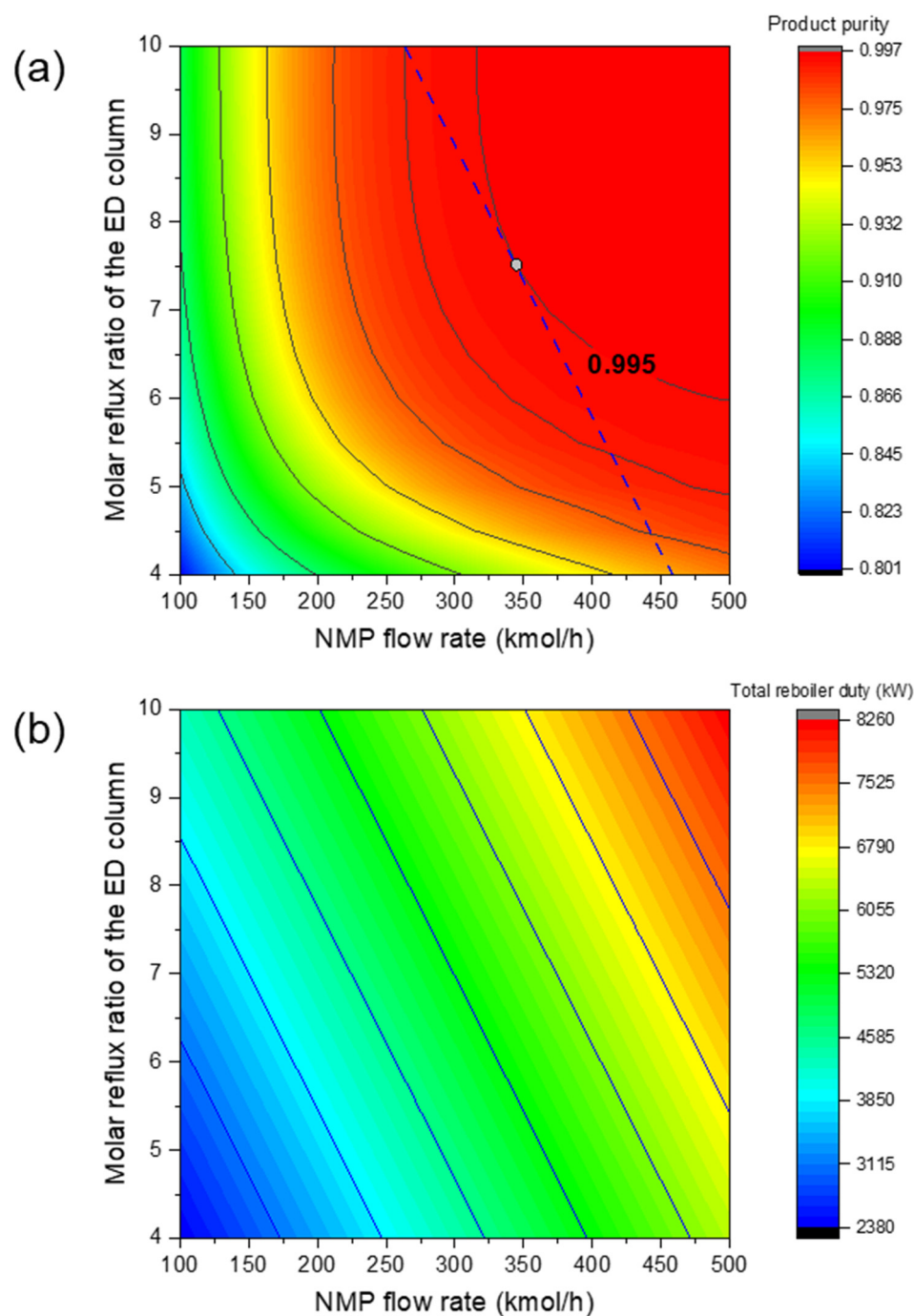


**Figure 6.** Influence of reflux ratio of the ED column and solvent usage on (a) product purity and (b) total reboiler duty for the NMP-based process.

After conducting the parameter sensitivity analysis, the energy consumptions at different operating conditions were calculated and hence the minimum energy consumption was identified. As shown in Figures 5a and 6a, the operating conditions for achieving the minimum energy consumption with purity constraint fulfilled are highlighted with the white circles. Table 2 summarizes the results of the optimized design parameters and total reboiler duty for comparison. As expected, the IL-based process was much more energy efficient. The total energy consumption was reduced by 26%. Figures 7 and 8 illustrate the optimal flowsheet of the ED processes using [PMIM][MCO] and NMP as the entrainer, respectively. As shown, the IL was regenerated completely for recycling, whereas a trace amount of solvent loss was observed for NMP.



**Table 2.** Optimized operating conditions and total energy consumptions of the ED process using NMP and [PMIM][MCO] as entrainers.

Entrainer	Solvent Usage (kmol/h)	Molar Reflux Ratio	Total Reboiler Duty (kW)
NMP	344.89	7.530	5940.1
[PMIM][MCO]	59.11	6.842	4360.8

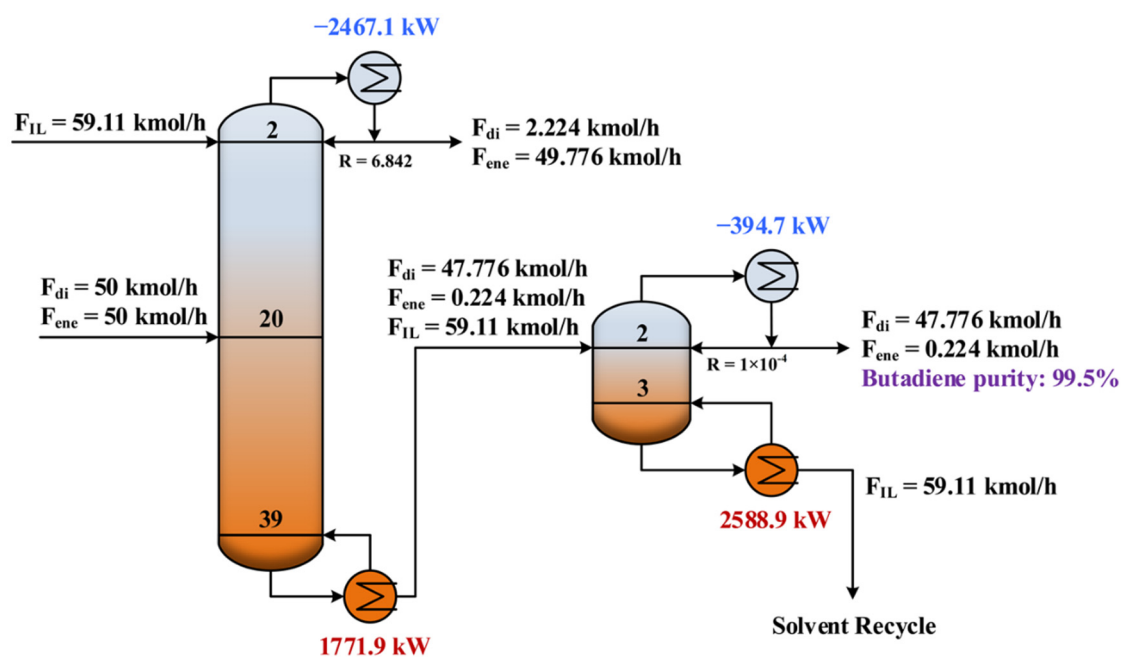


**Figure 7.** Optimal flowsheet of the ED process using [PMIM][MCO] as entrainer.

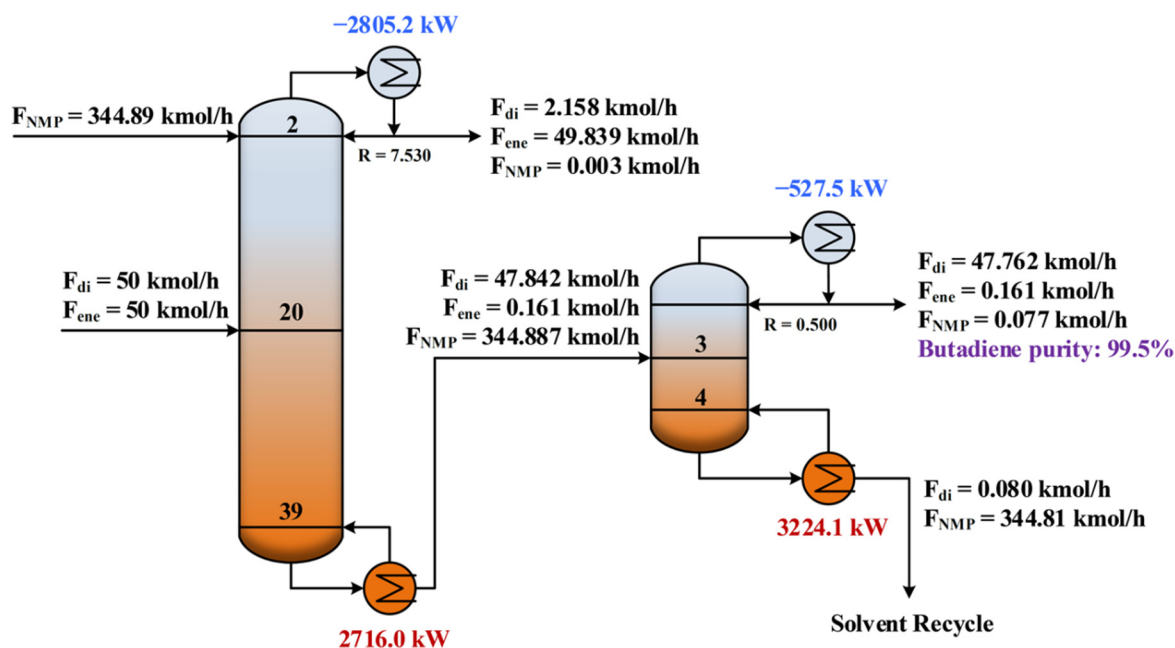


**Figure 8.** Optimal flowsheet of the ED process using NMP as entrainer.

### 3.4. $\sigma$ -Profile Analysis of [PMIM][MCO] and NMP

The  $\sigma$ -profile is one of the most important molecule-specific properties in the COSMO-RS, which is used to rationalize the high performance of IL [PMIM][MCO]. According to

the COSMO-RS theory, the non-polar region is centered at  $-0.0082 \text{ e}/\text{\AA}^2 < \sigma < 0.0082 \text{ e}/\text{\AA}^2$ . A broader distribution of  $\sigma$  outside the non-polar region usually reflects a higher polarity. Figure 9 depicts the  $\sigma$ -profiles of the cation and anion of [PMIM][MCO] as well as NMP. The cation [PMIM] shows a more pronounced peak in the non-polar region than NMP. This is also indicated by a larger amount of non-polar surface (green color). Such an observation can account for the increasing solvent power (i.e., capacity) of [PMIM][MCO] over NMP. Furthermore, compared with NMP in the polar region, the anion [MCO] presents a broader distribution. Again, this is affirmed by its large polar surface (red color). As a result, [PMIM][MCO] ultimately possesses quite high selectivity towards 1,3-C<sub>4</sub>H<sub>6</sub>. For better comparison, we have calculated the  $y$ - $x$  phase diagrams of {butadiene-butene-IL/NMP} by COSMO-RS at 298.15 K, shown in Figure 10. As seen, the relative volatility of 1-butene to 1,3-butadiene improved when the amount of solvent was increased. Moreover, comparing the two figures, it is found that the relative volatility of butene/butadiene with [PMIM][MCO] is larger than that using NMP as the solvent, which confirms that [PMIM][MCO] is a more promising entrainer than NMP for the butadiene/butene separation.

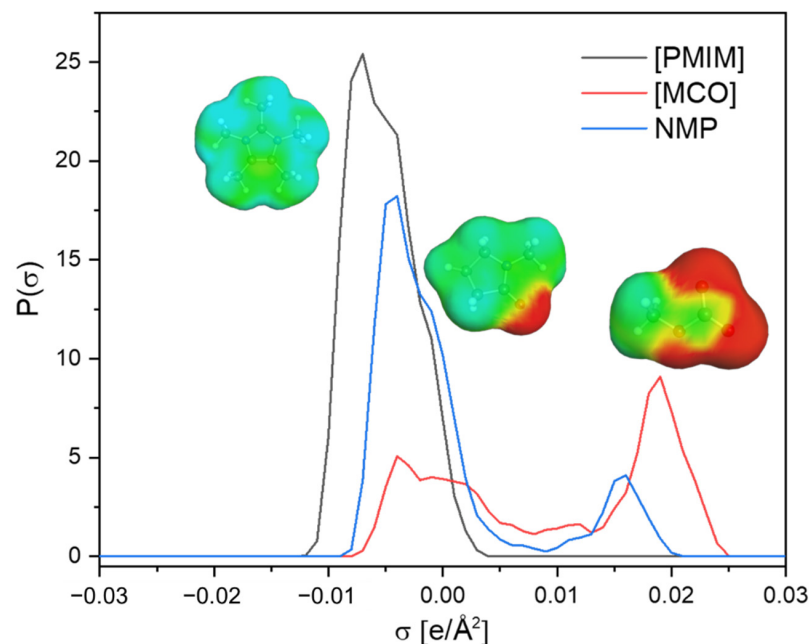


Figure 9.  $\sigma$ -Profile analysis of [PMIM][MCO] and NMP.

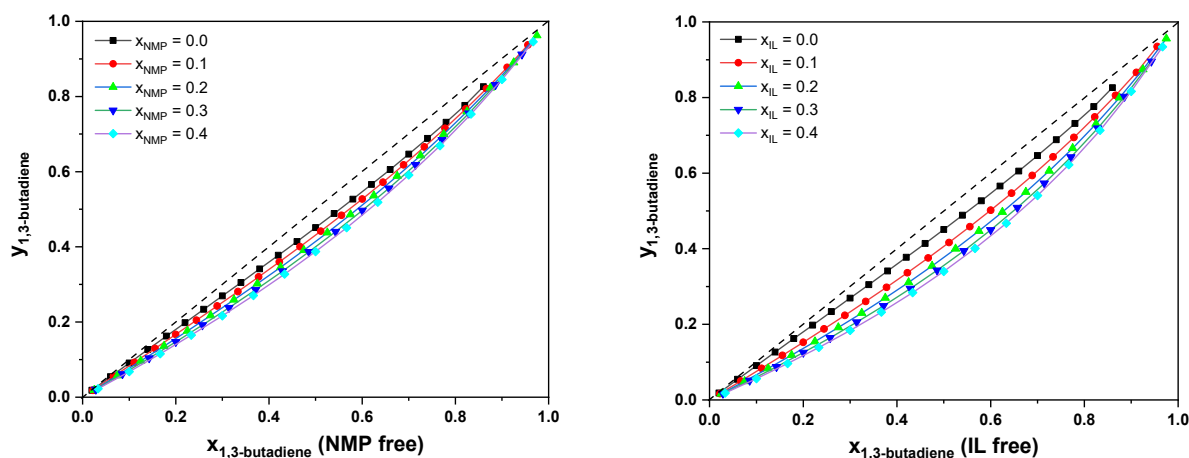


Figure 10. Vapor–liquid phase diagrams of {butadiene-butene-NMP} (left) and {butadiene-butene-[PMIM][MCO]} (right) at 298.15 K.

#### 4. Conclusions

In this work, the high-throughput computational screening of ionic liquids was performed in order to develop an energy-efficient extractive distillation process for separating 1,3-C<sub>4</sub>H<sub>6</sub> from C<sub>4</sub> hydrocarbon mixtures. First, the capacity and selectivity of 36,260 ILs (370 cations and 98 anions involved) at infinite dilution were calculated by COSMO-RS, and were filtrated with the reference of four organic solvents (i.e., NMP, DMF, DMSO and CAN). Accordingly, 190 out of the 36,260 ILs were retained. Secondly, three physical properties (i.e., viscosity, toxicity and melting point) of ILs were assessed by various models. Based on prespecified physical property constraints, a promising IL [PMIM][MCO] was identified. Finally, the process simulation of the remaining IL was conducted in Aspen Plus and its process performance was compared with the benchmark solvent NMP. In contrast with the NMP-based process, the energy consumption of using [PMIM][MCO] as entrainer was greatly reduced by 26%. As an additional rationalization, the  $\sigma$ -profiles of [PMIM][MCO] and NMP were analyzed and compared. They suggested that the combination of the highly non-polar cation [PMIM] and polar anion [MCO] may result in the high extraction performance of this IL.

**Supplementary Materials:** The following supporting information can be downloaded at: <https://www.mdpi.com/article/10.3390/pr10010165/s1>, Table S1: Information about the involved 370 cations and 98 anions; Table S2: COSMO-RS calculated thermodynamic performance of 36,260 ILs; Table S3: Prescreened 190 ILs to meet the thermodynamic criteria; Table S4: (a) The calculated viscosity of 190 ILs; (b) the calculated logEC50 of the 93 ILs that meet the viscosity constraint; (c) the calculated melting point of the 39 ILs that meet the toxicity constraint; Table S5: Necessary input information for Aspen Plus simulation employing the COSMO-SAC model. Information of the involved 370 cations and 98 anions; COSMO-RS calculated  $C^\infty$  and  $S^\infty$  of 36,260 ILs; IL physical property assessment including viscosity, toxicity and melting point; molecular input information for Aspen Plus simulation using the COSMO-SAC model (XLSX).

**Author Contributions:** Conceptualization: T.Z. and X.Z.; Methodology: T.Z. and H.Q.; Investigation: H.Q.; Writing—Original Draft Preparation: H.Q.; Writing—Review and Editing: Z.S., Z.W., X.Z. and T.Z. All authors have read and agreed to the published version of the manuscript.

**Funding:** This research was funded by Sino-German joint research project led by Deutsche Forschungsgemeinschaft (DFG) grant number SU 189/9-1 and National Natural Science Foundation of China (NSFC) grant number 21861132019.

**Institutional Review Board Statement:** Not applicable.

**Informed Consent Statement:** Not applicable.

**Data Availability Statement:** The data presented in this study are available on request from the corresponding author.

**Acknowledgments:** The authors gratefully acknowledge the support of the Sino-German joint research project led by Deutsche Forschungsgemeinschaft (DFG) and National Natural Science Foundation of China (NSFC) under the grants SU 189/9-1 and 21861132019, respectively. Teng Zhou acknowledges the financial support from the Max Planck Society to his Junior Professorship at OvGU Magdeburg dedicated to Computer-Aided Material and Process Design (CAMPD).

**Conflicts of Interest:** The authors declare that they have no known competing financial interests or personal relationships that could have appeared to influence the work reported in this paper.

#### References

1. Pomalaza, G.; Ponton, P.A.; Capron, M.; Dumeignil, F. Ethanol-to-butadiene: The reaction and its catalysts. *Catal. Sci. Technol.* **2020**, *10*, 4860–4911. [[CrossRef](#)]
2. Liao, P.Q.; Huang, N.Y.; Zhang, W.X.; Zhang, J.P.; Chen, X.M. Controlling guest conformation for efficient purification of butadiene. *Science* **2017**, *356*, 1193–1196. [[CrossRef](#)] [[PubMed](#)]
3. Coogler, W. New butadiene-recovery process. *Oil Gas J.* **1967**, *22*, 99–101.
4. Bannister, R.; Buck, E. Butadiene recovery via extractive distillation. *Chem. Eng. Prog.* **1969**, *65*, 65.

5. Tian, X.; Zhang, X.; Wei, L.; Zeng, S.; Huang, L.; Zhang, S. Multi-scale simulation of the 1, 3-butadiene extraction separation process with an ionic liquid additive. *Green Chem.* **2010**, *12*, 1263–1273. [\[CrossRef\]](#)
6. Lei, Z.; Zhou, R.; Duan, Z. Process improvement on separating C4 by extractive distillation. *Chem. Eng. J.* **2002**, *85*, 379–386. [\[CrossRef\]](#)
7. Lei, Z.; Wang, H.; Zhou, R.; Duan, Z. Solvent improvement for separating C4 with ACN. *Comput. Chem. Eng.* **2002**, *26*, 1213–1221. [\[CrossRef\]](#)
8. Mantingh, J.; Kiss, A.A. Enhanced process for energy efficient extraction of 1, 3-butadiene from a crude C4 cut. *Sep. Purif. Technol.* **2021**, *267*, 118656. [\[CrossRef\]](#)
9. Schulze, J.; Homann, M. Processes of Separation and Transformation in C4-Chemistry. In *C4-Hydrocarbons and Derivatives*; Springer: Berlin/Heidelberg, Germany, 1989; Volume 3, pp. 35–106.
10. Kindler, K.; Puhl, H. Method for Separating a C4-Hydrocarbon Mixture. Google Patents US6337429B1, 8 January 2002.
11. Wang, C.; Zhuang, Y.; Qin, Y.; Dong, Y.; Liu, L.; Zhang, L.; Du, J. Optimization and eco-efficiency analysis of extractive distillation processes with different solvents for separating the ternary mixture embedding two azeotropes. *Sep. Purif. Technol.* **2021**, *269*, 118763. [\[CrossRef\]](#)
12. Chai, S.; Song, Z.; Zhou, T.; Zhang, L.; Qi, Z. Computer-aided molecular design of solvents for chemical separation processes. *Curr. Opin. Chem. Eng.* **2022**, *35*, 100732. [\[CrossRef\]](#)
13. Yin, C.; Liu, G. Optimization of Solvent and Extractive Distillation Sequence Considering Its Integration with Reactor. *Processes* **2021**, *9*, 565. [\[CrossRef\]](#)
14. Song, Z.; Shi, H.; Zhang, X.; Zhou, T. Prediction of CO<sub>2</sub> solubility in ionic liquids using machine learning methods. *Chem. Eng. Sci.* **2020**, *223*, 115752. [\[CrossRef\]](#)
15. Zhang, X.; Wang, J.; Song, Z.; Zhou, T. Data-driven ionic liquid design for CO<sub>2</sub> capture: Molecular structure optimization and DFT verification. *Ind. Eng. Chem. Res.* **2021**, *60*, 9992–10000. [\[CrossRef\]](#)
16. Zhang, X.; Ding, X.; Song, Z.; Zhou, T.; Sundmacher, K. Integrated ionic liquid and rate-based absorption process design for gas separation: Global optimization using hybrid models. *AIChE J.* **2021**, *67*, e17340. [\[CrossRef\]](#)
17. Shi, H.; Zhang, X.; Sundmacher, K.; Zhou, T. Model-based optimal design of phase change ionic liquids for efficient thermal energy storage. *Green Energy Environ.* **2021**, *6*, 392–404. [\[CrossRef\]](#)
18. Dai, C.; Lei, Z.; Xi, X.; Zhu, J.; Chen, B. Extractive distillation with a mixture of organic solvent and ionic liquid as entrainer. *Ind. Eng. Chem. Res.* **2014**, *53*, 15786–15791. [\[CrossRef\]](#)
19. Shamsuri, A.A.; Daik, R. A succinct review on the PVDF/imidazolium-based ionic liquid blends and composites: Preparations, properties, and applications. *Processes* **2021**, *9*, 761. [\[CrossRef\]](#)
20. Shamsuri, A.A.; Jamil, S.N.A.M.; Abdan, K. Processes and properties of ionic liquid-modified nanofiller/polymer nanocomposites—A succinct review. *Processes* **2021**, *9*, 480. [\[CrossRef\]](#)
21. Karimi, B.; Tavakolian, M.; Akbari, M.; Mansouri, F. Ionic liquids in asymmetric synthesis: An overall view from reaction media to supported ionic liquid catalysis. *ChemCatChem* **2018**, *10*, 3173–3205. [\[CrossRef\]](#)
22. Lei, Z.; Dai, C.; Zhu, J.; Chen, B. Extractive distillation with ionic liquids: A review. *AIChE J.* **2014**, *60*, 3312–3329. [\[CrossRef\]](#)
23. Li, Q.; Zhang, J.; Lei, Z.; Zhu, J.; Zhu, J.; Huang, X. Selection of ionic liquids as entrainers for the separation of ethyl acetate and ethanol. *Ind. Eng. Chem. Res.* **2009**, *48*, 9006–9012. [\[CrossRef\]](#)
24. Díaz, I.; Palomar, J.; Rodríguez, M.; de Riva, J.; Ferro, V.; González, E.J. Ionic liquids as entrainers for the separation of aromatic-aliphatic hydrocarbon mixtures by extractive distillation. *Chem. Eng. Res. Des.* **2016**, *115*, 382–393. [\[CrossRef\]](#)
25. Stuckenholtz, M.; Crespo, E.A.; Vega, L.F.; Carvalho, P.J.; Coutinho, J.A.; Schröder, W.; Kiefer, J.; Rathke, B. Vapor liquid equilibria of binary mixtures of 1-butyl-3-methylimidazolium triflate (C<sub>4</sub>mimTfO) and molecular solvents: N-alkyl alcohols and water. *J. Phys. Chem. B* **2018**, *122*, 6017–6032. [\[CrossRef\]](#) [\[PubMed\]](#)
26. Song, Z.; Li, X.; Chao, H.; Mo, F.; Zhou, T.; Cheng, H.; Chen, L.; Qi, Z. Computer-aided ionic liquid design for alkane/cycloalkane extractive distillation process. *Green Energy Environ.* **2019**, *4*, 154–165. [\[CrossRef\]](#)
27. Huang, Y.; Ke, T.; Ke, Y.; Ren, Q.; Yang, Q.; Xing, H. Carboxylate ionic liquids with large free volume and strong hydrogen bonding basicity for efficient separation of butadiene and n-butene. *Ind. Eng. Chem. Res.* **2018**, *57*, 13519–13527. [\[CrossRef\]](#)
28. Camper, D.; Becker, C.; Koval, C.; Noble, R. Low pressure hydrocarbon solubility in room temperature ionic liquids containing imidazolium rings interpreted using regular solution theory. *Ind. Eng. Chem. Res.* **2005**, *44*, 1928–1933. [\[CrossRef\]](#)
29. Condemarin, R.; Scovazzo, P. Gas permeabilities, solubilities, diffusivities, and diffusivity correlations for ammonium-based room temperature ionic liquids with comparison to imidazolium and phosphonium RTIL data. *Chem. Eng. J.* **2009**, *147*, 51–57. [\[CrossRef\]](#)
30. Kilaru, P.K.; Condemarin, R.A.; Scovazzo, P. Correlations of low-pressure carbon dioxide and hydrocarbon solubilities in imidazolium-, phosphonium-, and ammonium-based room-temperature ionic liquids. Part Using surface tension. *Ind. Eng. Chem. Res.* **2008**, *47*, 900–909. [\[CrossRef\]](#)
31. Kilaru, P.K.; Scovazzo, P. Correlations of low-pressure carbon dioxide and hydrocarbon solubilities in imidazolium-, phosphonium-, and ammonium-based room-temperature ionic liquids. Part 2. Using activation energy of viscosity. *Ind. Eng. Chem. Res.* **2008**, *47*, 910–919. [\[CrossRef\]](#)
32. Anantharaj, R.; Banerjee, T. Quantum chemical studies on the simultaneous interaction of thiophene and pyridine with ionic liquid. *AIChE J.* **2011**, *57*, 749–764. [\[CrossRef\]](#)

33. Paduszynski, K.; Lukoshko, E.V.; Królikowski, M.; Domanska, U.; Szydłowski, J. Thermodynamic study of binary mixtures of 1-butyl-1-methylpyrrolidinium dicyanamide ionic liquid with molecular solvents: New experimental data and modeling with PC-SAFT equation of state. *J. Phys. Chem. B* **2015**, *119*, 543–551. [\[CrossRef\]](#) [\[PubMed\]](#)
34. Song, Z.; Zhang, C.; Qi, Z.; Zhou, T.; Sundmacher, K. Computer-aided design of ionic liquids as solvents for extractive desulfurization. *AIChE J.* **2018**, *64*, 1013–1025. [\[CrossRef\]](#)
35. Zhou, T.; Shi, H.; Ding, X.; Zhou, Y. Thermodynamic modeling and rational design of ionic liquids for pre-combustion carbon capture. *Chem. Eng. Sci.* **2021**, *229*, 116076. [\[CrossRef\]](#)
36. Yu, G.; Dai, C.; Lei, Z. Modified UNIFAC-Lei Model for Ionic Liquid-CH<sub>4</sub> Systems. *Ind. Eng. Chem. Res.* **2018**, *57*, 7064–7076. [\[CrossRef\]](#)
37. Paduszynski, K.; Domanska, U. Thermodynamic modeling of ionic liquid systems: Development and detailed overview of novel methodology based on the PC-SAFT. *J. Phys. Chem. B* **2012**, *116*, 5002–5018. [\[CrossRef\]](#)
38. Diedenhofen, M.; Eckert, F.; Klamt, A. Prediction of infinite dilution activity coefficients of organic compounds in ionic liquids using COSMO-RS. *J. Chem. Eng. Data* **2003**, *48*, 475–479. [\[CrossRef\]](#)
39. Ferreira, A.R.; Freire, M.G.; Ribeiro, J.C.; Lopes, F.M.; Crespo, J.G.; Coutinho, J.A. An overview of the liquid-liquid equilibria of (ionic liquid + hydrocarbon) binary systems and their modeling by the conductor-like screening model for real solvents. *Ind. Eng. Chem. Res.* **2011**, *50*, 5279–5294. [\[CrossRef\]](#)
40. Ferreira, A.R.; Freire, M.G.; Ribeiro, J.C.; Lopes, F.M.; Crespo, J.o.G.; Coutinho, J.o.A. Overview of the liquid-liquid equilibria of ternary systems composed of ionic liquid and aromatic and aliphatic hydrocarbons, and their modeling by COSMO-RS. *Ind. Eng. Chem. Res.* **2012**, *51*, 3483–3507. [\[CrossRef\]](#)
41. Anantharaj, R.; Banerjee, T. Aromatic sulfur-nitrogen extraction using ionic liquids: Experiments and predictions using an a priori model. *AIChE J.* **2013**, *59*, 4806–4815. [\[CrossRef\]](#)
42. Cheng, H.; Li, J.; Wang, J.; Chen, L.; Qi, Z. Enhanced vitamin E extraction selectivity from deodorizer distillate by a biphasic system: A COSMO-RS and experimental study. *ACS Sustain. Chem. Eng.* **2018**, *6*, 5547–5554. [\[CrossRef\]](#)
43. Paduszynski, K.; Królikowska, M. Extensive evaluation of performance of the COSMO-RS approach in capturing liquid-liquid equilibria of binary mixtures of ionic liquids with molecular compounds. *Ind. Eng. Chem. Res.* **2020**, *59*, 11851–11863. [\[CrossRef\]](#)
44. Paduszynski, K. An overview of the performance of the COSMO-RS approach in predicting the activity coefficients of molecular solutes in ionic liquids and derived properties at infinite dilution. *Phys. Chem. Chem. Phys.* **2017**, *19*, 11835–11850. [\[CrossRef\]](#) [\[PubMed\]](#)
45. Bezold, F.; Weinberger, M.E.; Minceva, M. Assessing solute partitioning in deep eutectic solvent-based biphasic systems using the predictive thermodynamic model COSMO-RS. *Fluid Phase Equilib.* **2017**, *437*, 23–33. [\[CrossRef\]](#)
46. Larriba, M.; de Riva, J.; Navarro, P.; Moreno, D.; Delgado-Mellado, N.; García, J.; Ferro, V.R.; Rodríguez, F.; Palomar, J. COSMO-based/Aspen Plus process simulation of the aromatic extraction from pyrolysis gasoline using the {[4empy][NTf<sub>2</sub>]+[emim][DCA]} ionic liquid mixture. *Sep. Purif. Technol.* **2018**, *190*, 211–227. [\[CrossRef\]](#)
47. Dai, C.; Dong, Y.; Han, J.; Lei, Z. Separation of benzene and thiophene with a mixture of *N*-methyl-2-pyrrolidinone (NMP) and ionic liquid as the entrainer. *Fluid Phase Equilib.* **2015**, *388*, 142–150. [\[CrossRef\]](#)
48. Yu, G.; Dai, C.; Gao, H.; Zhu, R.; Du, X.; Lei, Z. Capturing condensable gases with ionic liquids. *Ind. Eng. Chem. Res.* **2018**, *57*, 12202–12214. [\[CrossRef\]](#)
49. Sandler, S. Infinite dilution activity coefficients in chemical, environmental and biochemical engineering. *Fluid Phase Equilib.* **1996**, *116*, 343–353. [\[CrossRef\]](#)
50. Salleh, M.Z.M.; Hady-Kali, M.K.; Hashim, M.A.; Mulyono, S. Ionic liquids for the separation of benzene and cyclohexane-COSMO-RS screening and experimental validation. *J. Mol. Liq.* **2018**, *266*, 51–61. [\[CrossRef\]](#)
51. Eiden, P.; Bulut, S.; Köchner, T.; Friedrich, C.; Schubert, T.; Krossing, I. In silico predictions of the temperature-dependent viscosities and electrical conductivities of functionalized and nonfunctionalized ionic liquids. *J. Phys. Chem. B* **2011**, *115*, 300–309. [\[CrossRef\]](#)
52. Torrecilla, J.; Palomar, J.; Lemus, J.; Rodríguez, F. A quantum-chemical-based guide to analyze/quantify the cytotoxicity of ionic liquids. *Green Chem.* **2010**, *12*, 123–134. [\[CrossRef\]](#)
53. Peng, D.; Picchioni, F. Prediction of toxicity of ionic liquids based on GC-COSMO method. *J. Hazard. Mater.* **2020**, *398*, 122964. [\[CrossRef\]](#) [\[PubMed\]](#)
54. Wang, Z.; Song, Z.; Zhou, T. Machine learning for ionic liquid toxicity prediction. *Processes* **2021**, *9*, 65. [\[CrossRef\]](#)
55. Lazzús, J.A. A group contribution method to predict the melting point of ionic liquids. *Fluid Phase Equilib.* **2012**, *313*, 1–6. [\[CrossRef\]](#)
56. Huang, Y.; Dong, H.; Zhang, X.; Li, C.; Zhang, S. A new fragment contribution-corresponding states method for physicochemical properties prediction of ionic liquids. *AIChE J.* **2013**, *59*, 1348–1359. [\[CrossRef\]](#)